Ray Traces Through Unsteady Jet Turbulence

J. B. Freund
Theoretical and Applied Mechanics
University of Illinois at Urbana-Champaign
T. G. Fleischman
Mechanical and Aerospace Engineering
University of California, Los Angeles

Abstract

Results of an ongoing effort to quantify the role turbulence in scattering sound in jets are reported. Using a direct numerical simulation database to provide the flow data, ray paths traced through the mean flow are compared with those traced through the actual time evolving turbulent flow. Significant scattering by the turbulence is observed. The most notable effect is that upstream traveling waves that are trapped in the potential core by the mean flow, which acts as a wave guide, easily escape in the turbulent flow. A crude statistical estimate based on ray number density suggests that directivity is modified by the turbulence, but no rigorous treatment of non-uniformities in the high-frequency approximation is attempted.

Nomenclature

a	Sound speed
N	Number of rays observed
N_r	Number or rays released
M	Mach number
p	Pressure
Re	Reynolds number
r	Radial coordinate
r_o	Jet nozzle radius
s	Entropy
t	Time
u_i	Cartesian velocities ($i = 1, 2, 3$)
x	Axial coordinate
x_i	Cartesian coordinates
α	Directivity angle
ϕ	Wave phase
ρ	Density
θ	Cylindrical polar coordinate
ω	Angular frequency

Subscripts

j	Jet exit
∞	Ambient

Accents

$\overline{()}$	Base flow (potentially time dependent)

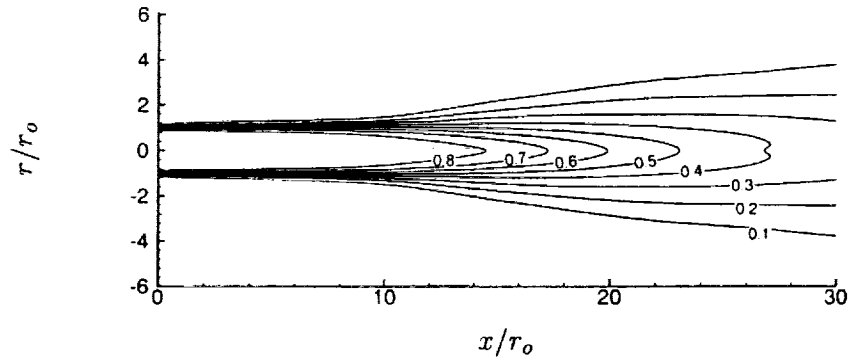

Figure 1: Contours of mean streamwise velocity: 8 evenly spaced contours from $0.1a_\infty$ to $0.8a_\infty$.

$()'$ Acoustic perturbation

1 Introduction

Lighthill's theory of aerodynamic noise is often criticized because it does not distinguish refraction from generation. Instead, these effects are grouped together in a nominal 'source':[1]

$$\underbrace{\frac{\partial^2 \rho}{\partial t^2} - a_\infty^2 \frac{\partial^2 \rho}{\partial x_j \partial x_j}}_{\text{sound propagation}} = \underbrace{\frac{\partial^2 T_{ij}}{\partial x_i \partial x_j}}_{\text{'source'}}, \tag{1}$$

where T_{ij} is the Lighthill stress tensor. Lighthill was, of course, aware of this but concluded that refraction "may affect finer details, but it does not appear to be fundamental."[2] It has since been argued that a distinction might not be necessary when developing predictive models,[3] but since generation and propagation are different physical processes, it is attractive to model them separately. Lighthill was not faced with the stringent noise regulations that we are today. With a great effort underway to achieve as little as a 3dB noise reduction, "finer details" are now more important. More recent but more complex acoustic analogies, such Lilley's equation,[4,5]

$$\underbrace{\frac{D}{Dt}\left(\frac{D^2\Pi}{Dt^2} - \frac{\partial}{\partial x_j}\left(a^2 \frac{\partial \Pi}{\partial x_j}\right)\right) + 2\frac{\partial u_k}{\partial x_j}\frac{\partial}{\partial x_k}\left(a^2 \frac{\partial \Pi}{\partial x_j}\right)}_{\text{sound propagation}}$$

$$= \underbrace{-2\frac{\partial u_j}{\partial x_k}\frac{\partial u_i}{\partial x_j}\frac{\partial u_k}{\partial x_i} + (\text{viscous terms})}_{\text{source}}, \tag{2}$$

attempt to better separate propagation and generation.

Unfortunately, since (2) is nonlinear it must be linearized for implementation and interpretation.[5] An estimate of the steady mean flow is typically chosen to linearize about and many ongoing modeling endeavors take this approach.[6,7] Even modelers that circumvent the exact governing equations as a starting point and designate a relatively *ad hoc* acoustic source[8] choose to linearize about a steady mean flow. To linearize the propagation operator in (2), the nonlinear terms can be omitted, which assumes they play no substantial role at all, or moved to the right hand side,

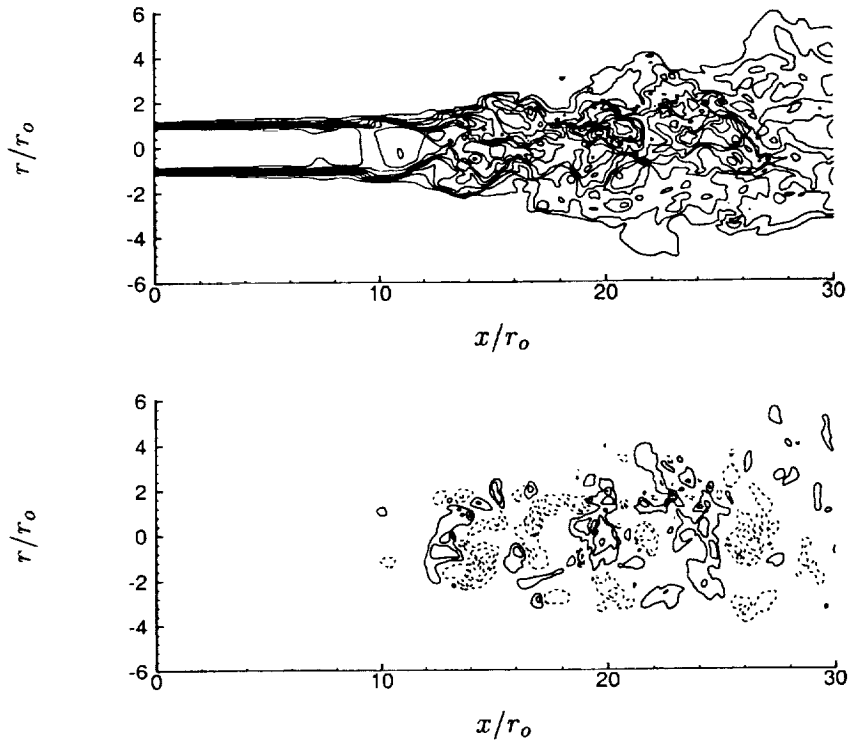

Figure 2: (a) Instantaneous axial velocity: 9 evenly spaced contours from $0.1a_\infty$ to $0.9a_\infty$. (b) Instantaneous radial velocity contours: $-0.3a_\infty$ to $0.3a_\infty$ with 0.1 spacing. Negative contours are dashed and the zero contour is omitted.

which is satisfying because the equation remains exact but once again blurs the distinction between source and propagation. Though convenient, linearization about the *mean* flow is well understood to be artificial since no individual sound wave actually encounters the mean flow.[9] Because local turbulence intensities can be over 100% in a jet, with large flow structures on the scale of the local jet radius, scattering by the turbulence might indeed be significant. We investigate this possibility.

Refraction in jets has been investigated on many fronts. In Mach 0.5 and 0.9 jets it was studied by MacGregor *et al.*[10] by adding an artificial noise source into the jets. Suzuki & Lele[11] used numerical methods and analysis to study both directional and frequency scattering of sound by instability waves in a two-dimensional mixing layer and showed a significant influence in some cases. While low frequency components of jet noise typically follow the Lighthill/Ffowcs Williams $I \propto (1 - M_c \cos\theta)^{-5}$ law, higher frequencies are less directive,[12] fit better by three inverse Doppler factors.[13] High-frequency solutions[14] of Lilley's equation for uni-directional transversely sheared flow might explain this, but scattering by turbulence has been offered as alternative explanation.[13] Similar high-frequency formulations have been incorporated into predictive tools[15,16] using a general high-frequency Green function derived by Durbin.[17] Adjoint Green functions have been proposed to simplify implementation of flow-acoustic interactions in models.[18]

The purpose of this ongoing study is to estimate the role of scattering by the unsteady turbulent fluctuations in a jet, and here we present a preliminary report on the effort. Since turbulence is analytically intractable, we rely on an existing, well-validated direct numerical simulation database to represent the turbulent jet flow. Flow-acoustic interaction is studied for high-frequency noise using an unsteady geometrical acoustic formulation to identify ray paths. Directivity is estimated statistically based on the ray paths, but no attempt has yet been made to construct instantaneous intensity profiles.

2 Simulation Database

Details of the direct numerical simulation database used in this study are reported in full elsewhere.[19–21] In summary, it is of a Reynolds number 3600, Mach number 0.9, temperature ratio $T_j/T_\infty = 0.86$ turbulent jet, which matches the experimental conditions studied by Stromberg *et al.*[22] Contours of mean streamwise velocity are shown in figure 1 and contours of instantaneous streamwise and radial velocity are shown in 2. At this Reynolds number, the initial shear layers are laminar as expected and thus qualitatively different from a high-Reynolds-number jet, which would have turbulent shear layers. However, after transition, which occurs a little before the potential core closes at $x \approx 14r_o$, the jet's development agrees well with those at a much higher Reynolds number data. Downstream of the potential core, the jet's spreading rate and Reynolds stresses agree with those of much higher Reynolds number jets.[21,23,24] This is important because it suggests that the energetic large scales are similar to those in jets at higher Reynolds numbers which should generalize the present results.

Other points of validation are reported elsewhere.[21] In these references it was shown that the mean flow, the noise directivity, and far-field noise spectrum are all in excellent agreement with the data of Stromberg *et al.*[22]

3 High-Frequency Approximation

High-frequency asymptotics will be used to study the interactions of sound with the flow. This approach is both convenient because it leads to tractable formulations, and important because the high frequencies are a particularly annoying component of the noise. Of course, the noise from a jet

at $Re = 3600$ is relatively narrow banded compared to jets at typical engineering Reynolds numbers. However, if we accept that the large, energy carrying turbulence scales are realistic, high-frequency noise sources can be artificially added to the flow in order study flow-acoustic interactions.

It is often found that high-frequency approximations give reasonable estimates for Helmholtz numbers as low as unity,[25-27] and we will use this to estimate a lower bound on the Strouhal numbers that might be accurately represented by our procedure. We take as our length scale the 50 percent two-point velocity correlation width of the turbulent eddies, which, depending on the location within the jet, is as low as $\ell \approx 0.5 r_o$.[21] This is smaller than the scale over which the mean flow varies (figure 1) except in the initial shear layers. Setting the Helmholtz number $He \equiv \omega \ell / a = 1$ gives $\omega \approx 2a/r_o$ or $St \equiv fD/U_j = \omega 2 r_o / 2\pi U_j \gtrsim 1.0$. Of course, the motion of the turbulent structures might decrease or increase their effective size for a particular sound wave they encounter. Assuming $M_c \approx 0.5$, this would potentially increase the Strouhal number limit by about one-third to 1.3, which is high but still relevant for many applications.

We develop an unsteady ray tracing formulation similar to that used by Colonius *et al.*[28] We start with the Euler equations in Cartesian coordinates and three space dimensions, with the energy equation written in terms of entropy,

$$\rho\left(\frac{\partial u_i}{\partial t} + u_j \frac{\partial u_i}{\partial x_j}\right) + \frac{\partial p}{\partial x_i} = 0 \tag{3}$$

$$\frac{\partial \rho}{\partial t} + u_j \frac{\partial \rho}{\partial x_j} + \rho \frac{\partial u_j}{\partial x_j} = 0 \tag{4}$$

$$\frac{\partial s}{\partial t} + u_j \frac{\partial s}{\partial x_j} = 0, \tag{5}$$

and decompose the dependent variables as

$$\begin{bmatrix} \rho \\ u_i \\ p \\ s \end{bmatrix}_{(x_i,t)} = \begin{bmatrix} \bar{\rho} \\ \bar{u}_i \\ \bar{p} \\ \bar{s} \end{bmatrix}_{(x_i,t)} + \begin{bmatrix} \rho' \\ u_i' \\ p' \\ s' \end{bmatrix}_{(x_i,t)}, \tag{6}$$

where $\overline{()}$ terms will be obtained from the simulation database and in general are functions of all space coordinates and time. The $()'$ terms are perturbations, but not necessarily acoustic at this point. Retaining only linear terms in the perturbations gives

$$\frac{\partial u_i'}{\partial t} + \bar{u}_j \frac{\partial u_i'}{\partial x_j} + u_j' \frac{\partial \bar{u}_i}{\partial x_j} + \frac{\rho'}{\bar{\rho}}\left(\frac{\partial \bar{u}_i}{\partial t} + \bar{u}_j \frac{\partial \bar{u}_i}{\partial x_j}\right) + \frac{1}{\bar{\rho}} \frac{\partial p'}{\partial x_i} = 0 \tag{7}$$

$$\frac{\partial \rho'}{\partial t} + \bar{u}_j \frac{\partial \rho'}{\partial x_j} + \bar{\rho} \frac{\partial u_j'}{\partial x_j} + \rho' \frac{\partial \bar{u}_j}{\partial x_j} + u_j' \frac{\partial \bar{\rho}}{\partial x_j} = 0 \tag{8}$$

$$\frac{\partial s'}{\partial t} + \bar{u}_j \frac{\partial s'}{\partial x_j} + u_j' \frac{\partial \bar{s}}{\partial x_j} = 0. \tag{9}$$

We next assume harmonic fluctuations

$$\begin{bmatrix} u_i' \\ \rho' \\ p' \\ s' \end{bmatrix} = \begin{bmatrix} U_i \\ R \\ P \\ S \end{bmatrix} e^{i\omega\phi(x_i,t)}, \tag{10}$$

where U_i, R, P and S are complex amplitudes that are functions of (x_i, t), ϕ is a real-valued phase function, and ω is the (large) angular frequency of the disturbances. Substituting and retaining only the highest order terms in ω yields

$$\left(\frac{\partial\phi}{\partial t} + \bar{u}_j\frac{\partial\phi}{\partial x_j}\right)U_i + \frac{\bar{p}}{\bar{\rho}}\frac{\partial\phi}{\partial x_i}S + \frac{\bar{a}^2}{\bar{\rho}}\frac{\partial\phi}{\partial x_i}R = 0 \tag{11}$$

$$\left(\frac{\partial\phi}{\partial t} + \bar{u}_j\frac{\partial\phi}{\partial x_j}\right)R + \bar{\rho}\frac{\partial\phi}{\partial x_j}U_j = 0 \tag{12}$$

$$\left(\frac{\partial\phi}{\partial t} + \bar{u}_j\frac{\partial\phi}{\partial x_j}\right)S = 0. \tag{13}$$

This leaves 5 equations and 5 unknowns. For a non-trivial solution the determinant of this system must be zero:

$$G^3\left[G^2 - \bar{a}^2\left(\frac{\partial\phi}{\partial x_j}\frac{\partial\phi}{\partial x_j}\right)\right] = 0, \tag{14}$$

where $G = \frac{\partial\phi}{\partial t} + \bar{u}_j\frac{\partial\phi}{\partial x_j}$. It is obvious that $G^3 = 0$ roots correspond to vorticity and entropy modes and are therefore not of concern to us. The remaining equation can be solved by method of characteristics to yield a system of ordinary differential equations for the ray paths,

$$\frac{dx_i}{dt} = \bar{u}_i - \frac{\bar{a}^2\phi_{x_i}}{\phi_t + \bar{u}_j\phi_{x_j}} \tag{15}$$

$$\frac{d\phi_{x_i}}{dt} = -\frac{\partial\bar{u}_j}{\partial x_i}\phi_{x_j} + \frac{\partial\bar{a}^2}{\partial x_i}\frac{\phi_{x_j}\phi_{x_j}}{\phi_t + \bar{u}_j\phi_{x_j}} \tag{16}$$

$$\frac{d\phi_t}{dt} = -\frac{\partial\bar{u}_j}{\partial t}\phi_{x_j} + \frac{\partial\bar{a}^2}{\partial t}\frac{\phi_{x_j}\phi_{x_j}}{\phi_t + \bar{u}_j\phi_{x_j}} \tag{17}$$

$$\frac{d\phi}{dt} = 0, \tag{18}$$

where subscripts on ϕ indicate partial differentiation.

Once an initial coordinate is chosen, initial conditions for ϕ_{x_i} are determined by solving (15) with $\phi_t = r_o/a_\infty$ and

$$\frac{d}{dt}\begin{bmatrix}x_1\\x_2\\x_3\end{bmatrix} = \begin{bmatrix}\bar{a}\cos\alpha + \bar{u}_1\\ \bar{a}\sin\alpha\cos\theta + \bar{u}_2\\ \bar{a}\sin\alpha\sin\theta + \bar{u}_3\end{bmatrix}. \tag{19}$$

The results are insensitive to the choice of ϕ_t and, as we shall see, (17) in general.

4 Procedure

Equations (15) through (18) were integrated using a fourth-order Runge–Kutta algorithm with $\Delta t = 0.01 r_o/a_\infty$. Coefficients $\bar{u}_i$ and $\bar{a}$ were taken from the direct numerical simulation database. This data was available every $\Delta t = 0.17 r_o/a_\infty$ and at every other mesh point of the original computation. It was interpolated in space using B-splines and in time using a linear method. Differences were computed using second-order centered finite differences with $\delta = 0.001 r_o$. Results were insensitive to this value and did not change if a fourth-order finite difference was used instead. Results were also insensitive to the order of the B-spline used. We traced $N_r = 1000$ rays through the mean-flow and $N_r = 500$ rays through the unsteady flow. They were initially directed at evenly spaced α-angles in the $\theta = 0, \pi$ and $\theta = \pm\pi/2$ planes (see figure 3). Results shown here were

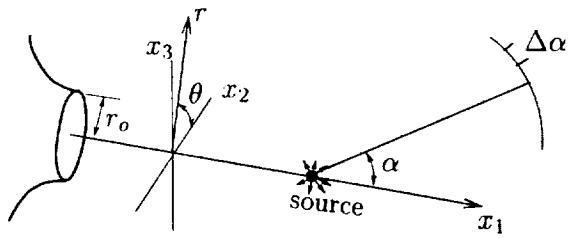

Figure 3: Coordinate system schematic.

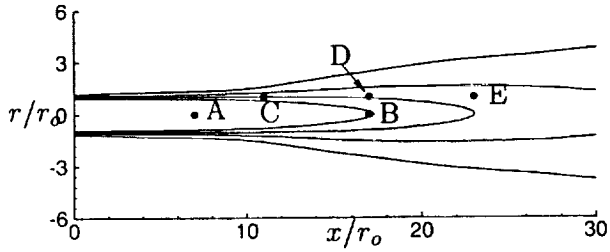

Figure 4: Schematic showing source points used. See also table 1.

insensitive to the number of rays traced. Except when noted, rays were traced for a total time of $25.5r_o/a_\infty$.

Focusing by the turbulence will cause ray path to cross at points in their trajectories. At these caustics, the high-frequency approximation for amplitude, which can be obtained from the next highest terms in ω, fails because the wave fronts develop cusps, a feature that is always small with respect to a wavelength of the sound. In addition, behind the caustics multiple rays pass through each point and potentially interfere with each other. Even in a steady case with simply defined caustics, a rigorous solution in regions of multiple rays adds considerable complexity. In the present case where caustics are numerous, transitory and impossible to anticipate, we have not undertaken the task of developing a uniformly valid amplitude procedure. Instead, to estimate the effect of refraction on directivity we simply count the number of rays passing through different regions on a sphere surrounding the source. The resulting ray number density, N, can be shown inversely related to ray tube area, A, and thus proportional to tube intensity, I, which is valid where there are no caustics. We assume that the volume of the caustic-affected region crossing the observation sphere is negligible and the positions of the caustics ever changing, as is indeed observed, and can

CASE	x/r_o	r/r_o
A	7	0
B	17	0
C	11	1
D	17	1
E	23	1

Table 1: Source points (see figure 4). All have $\theta = 0$.

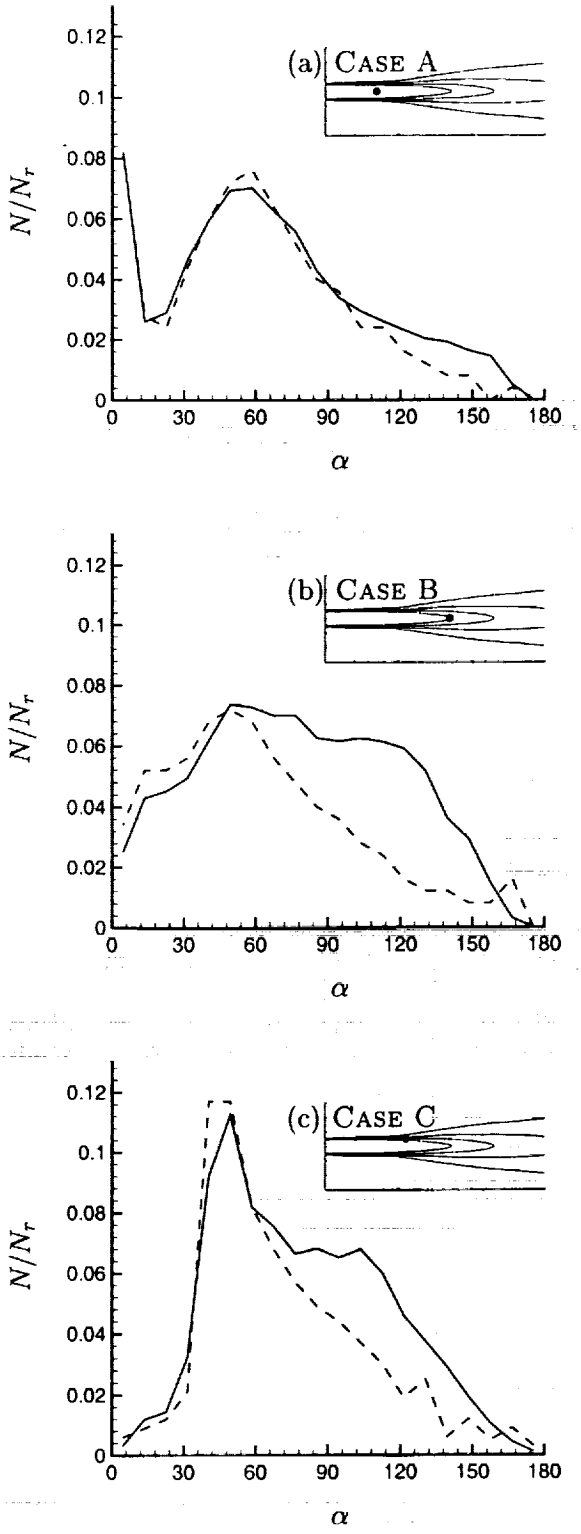

Figure 5: Figure continues on the following page.

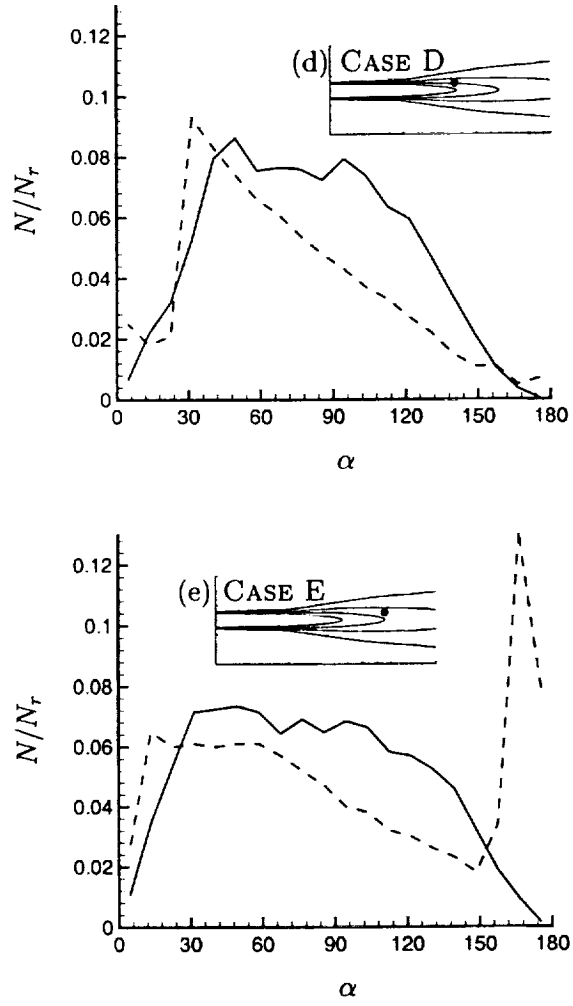

Figure 5: (a-e) Bin number density for rays traced through mean ---- and turbulent —— jet flows. See table 1 for source points.

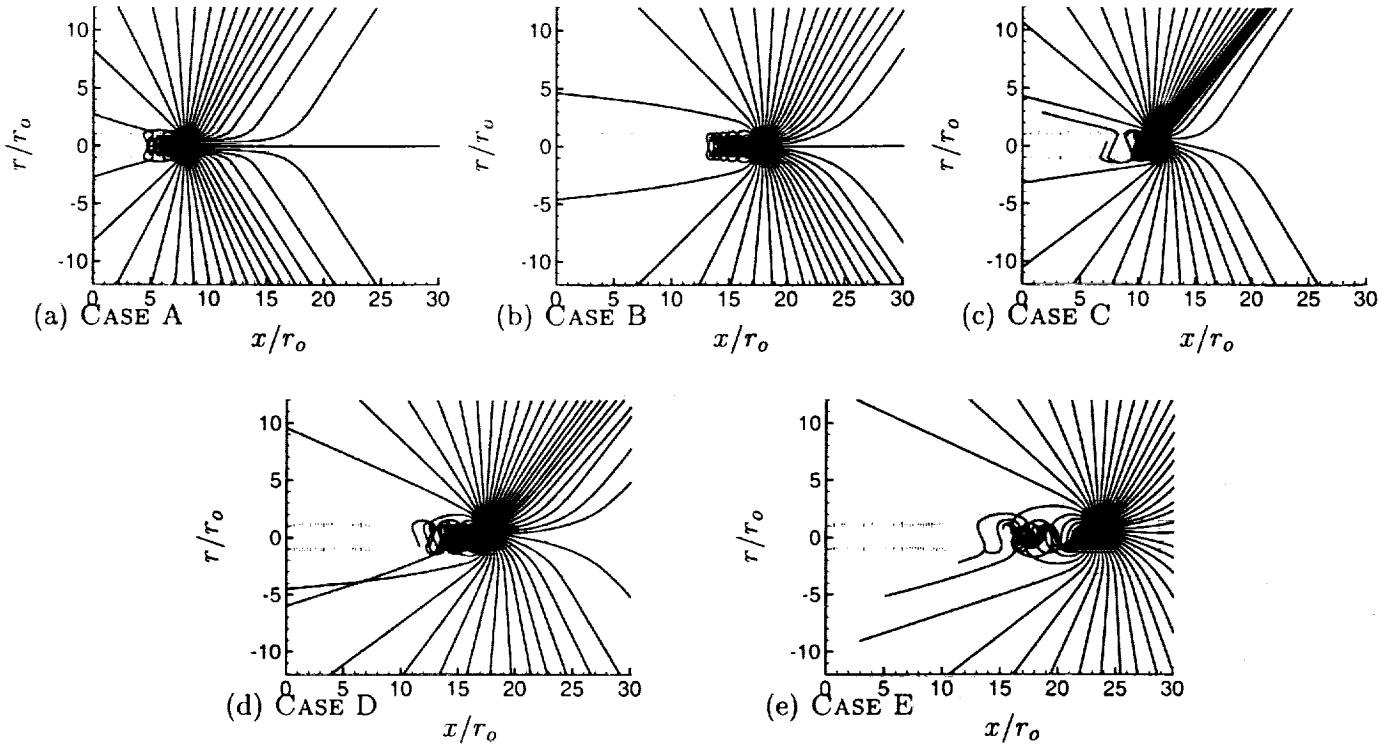

Figure 6: Every tenth ray path released in the x-y plane in the mean flow for labeled cases (see table 1).

therefore neglect them in the statistical average. We also assume that behind the caustics the rays are decorrelated due to the stochastic action of the turbulence so we also neglect interference. The results of these assumptions is a statistical beam-like method which provides an estimate of directivity.

Ray position statistics were accumulated as they exited a sphere of radius $r = 6.0r_o$ centered on the jet axis closest to the source. Monitoring a sphere at $r = 10r_o$ instead of $r = 6.0r_o$ caused a negligible change in our results. These data were collected in 20 bins of width $\Delta\alpha$ (see figure 3). Some rays were trapped in the jet, usually in the initial shear layers that act as a wave guide, and did not reach this spherical surface in the run time. These rays were not counted on the assumption they would have dissipated or entered the nozzle. Using a run time of $10r_o/a_\infty$ did not change the directivity estimates for $\alpha \lesssim 150°$. For the unsteady case, rays were traced through 39 separate time series that were separated in initial times by at least one large-eddy turnover time. The turbulence evolved as the rays progressed.

5 Results and Conclusions

The five point-source positions studied are labeled in figure 4 and summarized in table 1. The ray number-density directivities for all cases are plotted in figure 5 (a-e). In figure 5 (a), where the source is in the laminar potential core region ($x = 7r_o, r = 0$), we see little difference between the steady and unsteady ray number-density directivity. However, for rays released on the jet's axis just past the end of the potential core at $x = 17r_o$ (figure 5 b), there is a significant difference between the two cases. In the mean-flow case, substantially fewer rays leave the observation sphere

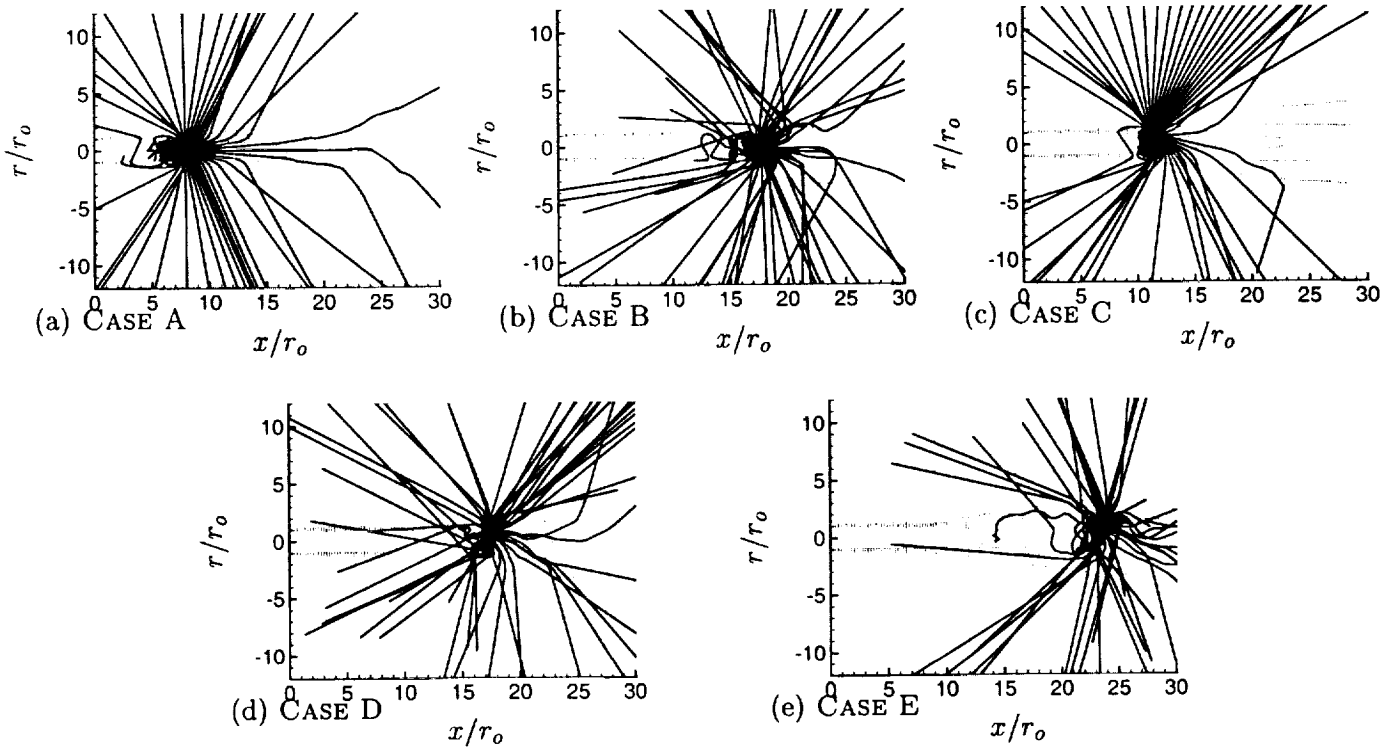

Figure 7: Every fifth ray released in the x–y plane in the unsteady flow for the labeled cases (see table 1).

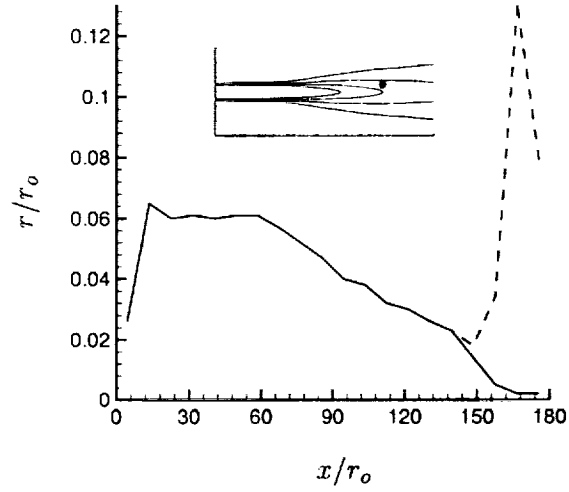

Figure 8: Mean flow ray number-density directivity for trace times of $10r_o/a_\infty$ —— and $25r_o/a_\infty$ ---- . CASE E is shown.

at angles greater than $\alpha = 70°$. The reason for this is clear in figure 6 (b): the upstream traveling waves are trapped by the jet's shear layers. However, in the unsteady case the rays escape and radiate as seen in figure 7 (b). Other source points are seen to give similar results.

The freeing of trapped rays appears to be the principle difference between the steady and unsteady cases for all the source points considered. In figure 5 (e), the upstream velocity is slow enough that trapped upstream traveling waves appear as a spike in the profile near $\alpha = 180°$ at the observation time. The trapped rays must eventually escape or enter the nozzle. Whether they will eventually affect the directivity is unclear, but the rate of release is slow: the steady-flow number-density directivity is unchanged for ray trace times of $10r_o/a_\infty$ versus $25r_o/a_\infty$ for $\alpha \lesssim 150°$ (see figure 8). If they do eventually leave the jet, they will do so differently than the rays in a realistic turbulent jet.

So far we have assumed that the source itself has no inherent directivity. However, if the sources are convecting quadrupoles, this is not true. In figures 9 (a-e) the rays have been given an initial weighting so that they would have a three Doppler factor, $W^{-3} = (1 - M_c \cos\alpha)^{-3}$, directivity in absence of additional refraction. The convection Mach number was taken to be $M_c = 0.5$, which corresponds to a convection velocity of $U_c = 0.6U_j$. We again see significant influence of the turbulence on the directivity estimates.

It is interesting to estimate how much of the scattering is because of the presences of the turbulence at any instance in time versus its change in time. To this end we have plotted a directivity for case B with the time derivative terms of the background flow in (18) set to zero. We compare with the correct equation results in figure 10, and see that there is an effect for $\alpha \gtrsim 60°$, but not a large one. It appears that accounting for the turbulence as a succession of steady states would provide most of the scattering.

In summary, we have made a crude estimate of the effect of turbulence on the propagation of high-frequency noise in turbulent jets and found that turbulence does affect the ray number density on a spherical surface outside the jet, increasing it in most cases. The most significant mechanism observed was that the turbulence frees rays that would otherwise be trapped traveling upstream in the potential core if only refraction by the mean flow were considered. The spatial variation of the turbulence was found to be more an influence on scattering than its time evolution.

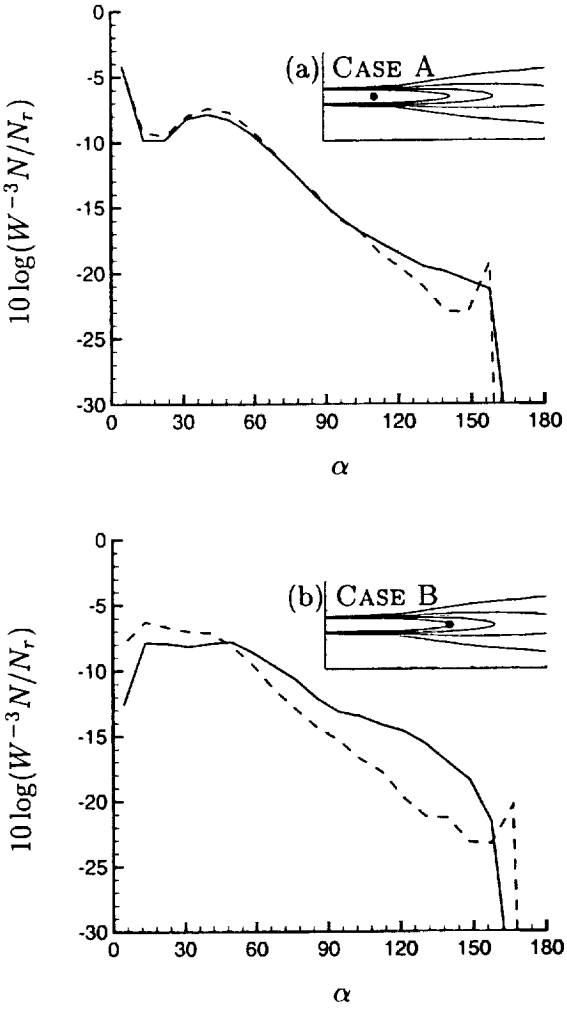

Figure 9: Figure continues on page 9.

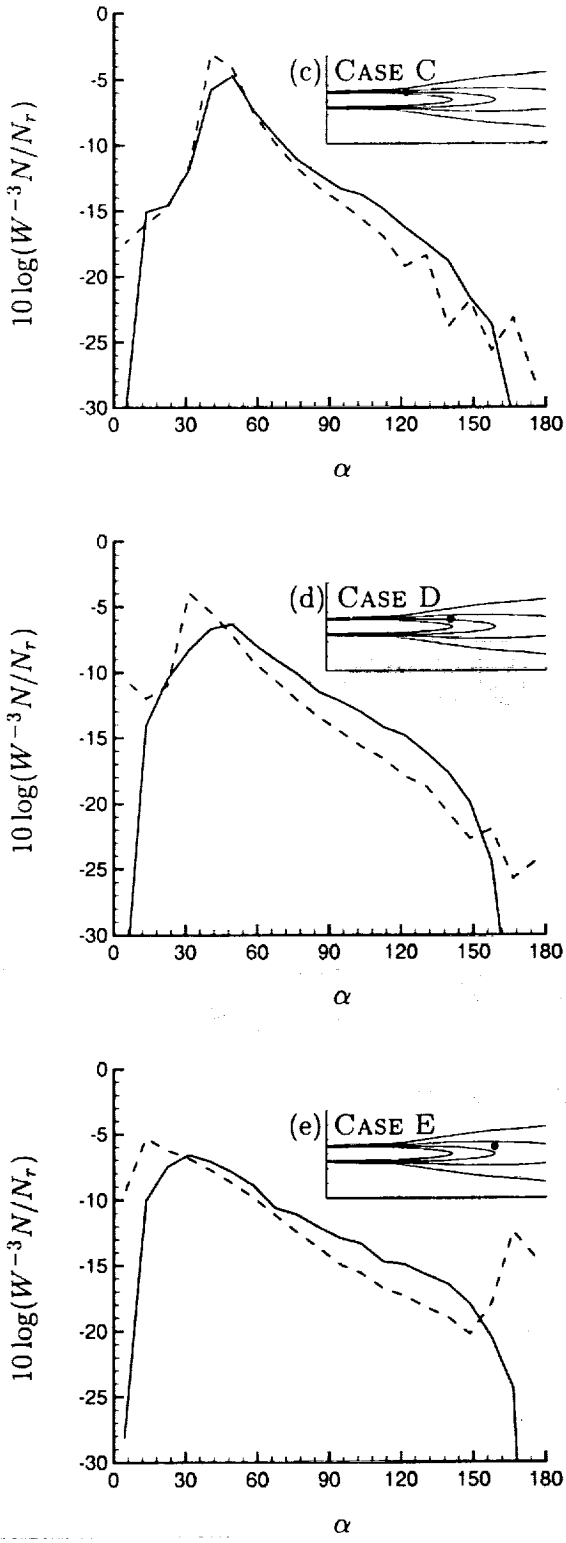

Figure 9: (a-e) Directivity when rays are given an effective three Doppler factors weighting.

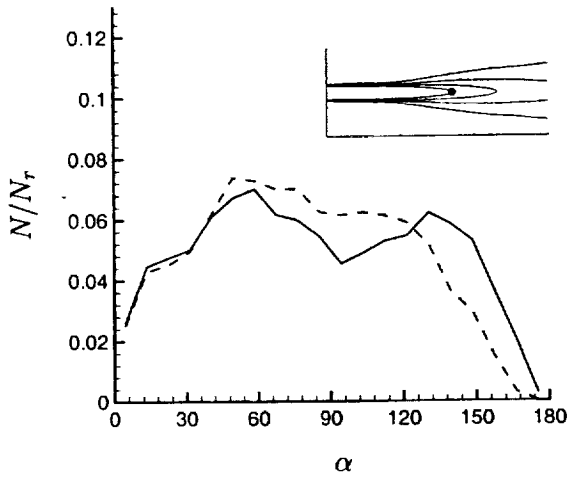

Figure 10: Directivity for CASE B, $x = 17r_o, r = 0$, with time derivatives in (17) ---- and without ——— .

This work is ongoing and a rigorous means of computing directivity as well as more realistic sources are being considered.

Acknowledgments

Support for this work provided by NASA is very gratefully acknowledged.

References

[1] Lighthill, M. J., "On sound generated aerodynamically: I. General theory," *Proc. Royal Soc. Lond. A*, Vol. 211, 1952, pp. 564–587.

[2] Lighthill, M. J., "On sound generated aerodynamically: II. Turbulence as a source of sound," *Proc. Royal Soc. Lond. A*, Vol. 222, 1954, pp. 1–32.

[3] Bailly, C., Lafon, P., and Candel, S., "Computation of subsonic and supersonic jet mixing noise using a modified k–ε model for compressible free shear flows," *Acta Acustica*, Vol. 2, 1994, pp. 101–112.

[4] Lilley, G. M., "On the noise from jets," Tech. Rep. CP-131, AGARD, 1974.

[5] Goldstein, M. E., *Aeroacoustics*, McGraw-Hill Book Co., 1976.

[6] Khavaran, A., Krejsa, E. A., and Kim, C. M., "Computation of supersonic jet mixing noise for an axisymmetric convergent-divergent nozzle," *J. Aircraft*, Vol. 31, 1994, pp. 603–609.

[7] Khavaran, A., "Role of anisotropy in turbulent mixing noise," *AIAA J.*, Vol. 37, No. 7, 1999, pp. 832–841.

[8] Tam, C. K. W. and Auriault, L., "Jet mixing noise from fine-scale turbulence," *AIAA J.*, Vol. 37, No. 2, 1999, pp. 145–153.

[9] Dowling, A. P., Ffowcs Williams, J. P., and Goldstein, M. E., "Sound propagation in a moving stream," *Phil. Trans. Roy. Soc. Lond. A*, Vol. 288, No. 1353, March 1978, pp. 321 349.

[10] MacGregor, G. R., Ribner, H. S., and Lam, H., "'Basic' jet noise patterns after delection of convection and refractioneffects: experiments vs. theory," *J. of Sound and Vib.*, Vol. 27, No. 4, 1973, pp. 437-454.

[11] Suzuki, T. and Lele, S. K., "Acoustic scattering from a mixing layer: role of instability waves," AIAA Paper 99-0228, 1999.

[12] Lush, P. A., "Measurements of subsonic jet noise and comparison with theory," *J. Fluid Mech.*, Vol. 46, 1971, pp. 477–500.

[13] Goldstein, M. E., "Aeroacoustics of turbulent shear flows," *Ann. Rev. Fluid Mech.*, Vol. 16, 1984.

[14] Goldstein, M. E., "High frequency sound emission from moving point multipole sources embedded in arbitrary transversely sheared mean flows," *J. of Sound and Vib.*, Vol. 80, No. 4, 1982, pp. 499–522.

[15] Khavaran, A. and Krejsa, E. A., "Propagation of high frequency jet noise using geometric acoustics," 31st Aerospace Sciences Meeting, Reno, NV, AIAA Paper 93-0147, January 1993.

[16] Khavaran, A. and Krejsa, E. A., "Refraction of high frequency jet noise in an arbitrary jet flow," 32nd Aerospace Sciences Meeting, Reno, NV, AIAA Paper 93-0147, January 1994.

[17] Durbin, P. A., "High frequency Green function for aerodynamic noise in moving media, Part 1: General Theory," *J. of Sound and Vib.*, Vol. 91, No. 4, 1983, pp. 519–525.

[18] Tam, C. K. W. and Auriault, L., "Mean flow refraction effects on sound radiated from localized sources in a jet," *J. Fluid Mech.*, Vol. 370, 1998, pp. 149–174.

[19] Freund, J. B., "Direct numerical simulation of the noise from a Mach 0.9 jet," ASME FEDSM99-7251, 1999.

[20] Freund, J. B., "Acoustic sources in a turbulent jet: a direct numerical simulation study," AIAA Paper 99-1858, 1999.

[21] Freund, J. B., "Noise sources in a low-Reynolds-number turbulent jet at Mach 0.9," *J. Fluid Mech.*, Vol. 438, 2001, pp. 277–305.

[22] Stromberg, J. L., McLaughlin, D. K., and Troutt, T. R., "Flow field and acoustic properties of a Mach number 0.9 jet at a low Reynolds number," *J. of Sound and Vib.*, Vol. 72, No. 2, 1980, pp. 159–176.

[23] Hussein, H. J., Capp, S. P., and George, W. K., "Velocity measurements in a high-Reynolds-number, momentum-conserving, axisymmetric, turbulent jet," *J. Fluid Mech.*, Vol. 258, 1994, pp. 31-75.

[24] Panchapakesan, N. R. and Lumley, J. L., "Turbulence measurements in axisymmetric jets of air and helium. Part 1. Air jets," *J. Fluid Mech.*, Vol. 246, 1993, pp. 197–223.

[25] Balsa, T. F., "The far field of high frequency convected singularities in sheared flows, with application to jet noise prediction," *J. Fluid Mech.*, Vol. 74, 1976, pp. 193-208.

[26] Tester, B. J. and Morfey, C. L., "Developments in jet noise modeling - theoretical predicitons and comparisons with measured data," *J. of Sound and Vib.*, Vol. 46, No. 1, 1976, pp. 79–103.

[27] Scott, J. N., "Propagation of sound waves through linear shear layers," *AIAA J.*, Vol. 17, 1979, pp. 237–244.

[28] Colonius, T., Lele, S. K., and Moin, P., "The scattering of sound waves by a compressible vortex–numerical simulations and analytical solutions," *J. Fluid Mech.*, Vol. 260, 1994, pp. 271–409.